HASP 2012 Final Science Report and Failure Analysis

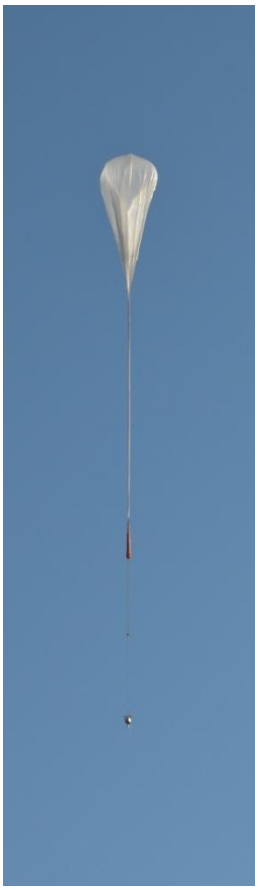

Montana State University

Payload 04

“Single Event Effect Detector”

December 14, 2012

MONTANA
STATE UNIVERSITY
Mountains & Minds

Table of Contents

I. Introduction

The Single Event Effect Detector has been designed and developed as part of ongoing research at the Montana State University High-Speed Digital Design Lab in Bozeman, Montana. The overarching goal of this research is to demonstrate a radiation-tolerant, SRAM-based FPGA computer system capable of operation in harsh terrestrial or space radiation environments. As with most electronics designed for these types of applications, this system seeks to mitigate single event effects caused by the interactions between ionizing radiation and modern electronics. "Single event effects" is an umbrella term for several possible scenarios involving these interactions. As a high-energy particle passes through a semiconductor material it leaves behind a charge track consisting of electron-hole pairs. In the context of the affected electronic system, the recombination of this excess charge represents an errant electrical current. A single event transient (SET) occurs when this current flows in such a way as to cause a transistor to temporarily change state. If perchance this erroneous transient state is latched into a memory element within the system, a single event upset (SEU) occurred. The behavior of SRAM-based FPGAs is determined by radiation susceptible memory contents. An SEU occurring within this memory changes the functionality of the underlying hardware, and is known as a single event functional interrupt (SEFI). Many techniques exist for mitigating these effects. These techniques frequently combine shielding with redundant hardware systems wherein the shielding reduces the amount of radiation that reaches the sensitive electronic components and the redundant hardware prevents errors from propagating through the computer system. Additionally, manufacturing processes may be used to increase radiation tolerance at the chip level often at the expense of circuit performance and higher cost. The flexibility of FPGAs can be leveraged to implement radiation tolerant architectures on-chip using coarse-grained triple modular redundancy (TMR) along with majority-rules voting. Readback scrubbing of the configuration memory combined with the ability to dynamically reconfigure regions within the FPGA at runtime can be used to enhance radiation tolerance.

The effects of ionizing radiation are largely absent on the earth's surface due to the combined shielding of the magnetosphere and atmosphere. This makes testing radiation tolerant computer architectures difficult due to the lack of single event effects. There are only a handful of ways to test space-bound systems on earth. Sophisticated high-energy pulsed laser systems and particle accelerators, both of which are expensive and pose logistical difficulties when testing electronic components, are among the testing options. High-altitude scientific balloons offer a unique platform for testing radiation effects. Though the radiation levels in the near-space atmosphere are lower than would be found in space, they tend to be significantly higher than on earth's surface. Scientific

balloons enable systems to be tested in harsh radiation environments for longer durations than suborbital launch vehicles, and, in the case of the HASP program, at significantly reduced cost.

The payload designed for the HASP 2012 flight was a first-generation general purpose test platform for FPGA-based radiation-tolerant computer architectures. The payload electronics consisted of a custom printed circuit board stack. The circuit boards populated for flight included a power supply board, an FPGA computer board, and a radiation sensor board. In addition to serving as a radiation tolerant hardware test platform, the FPGA board was a data logger for the radiation sensor. The sensor was a custom silicon strip sensor which was designed and built in-house by researchers at Montana State University. The 18-mm x 18-mm sensor is comprised of 16 front-side detection channels and 16 back-side detection channels. The front- and back-side channels are oriented orthogonally to create a 256-intersection grid. The sensor outputs were monitored by high-speed sampling logic within an FPGA.

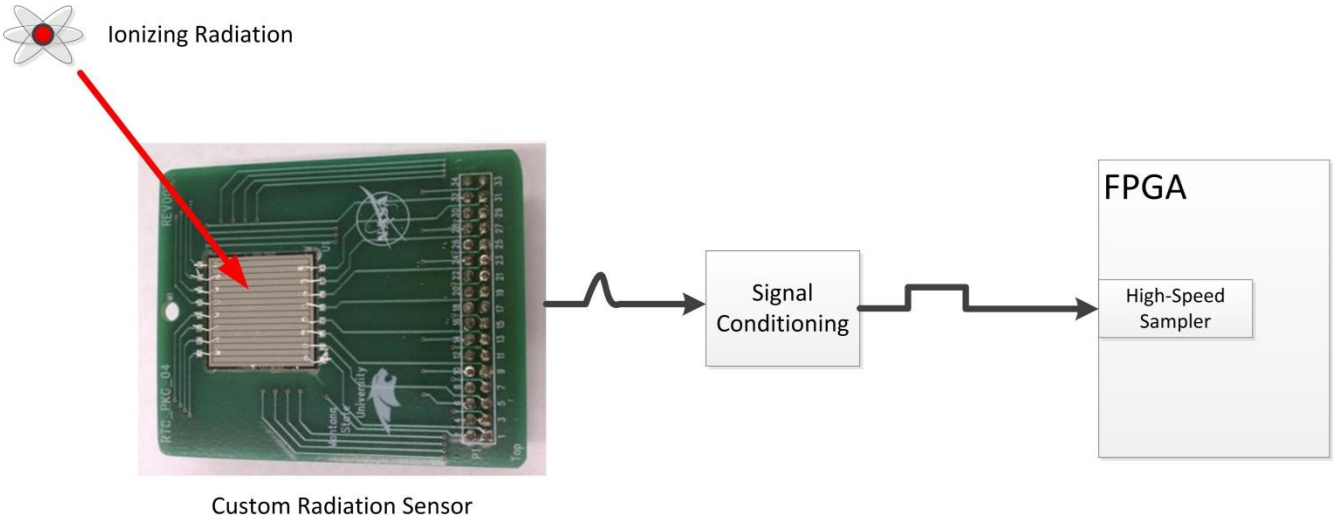

Figure 1- Radiation sensor signal path

The radiation sensor was designed for inclusion in the PCB stack in order to provide an environmental awareness to control-elements of the computer architecture. This is meant to help detect and prioritize the repairing of faults. The sensor was not used in this feedback capacity on the 2012 flight. This report details the science objectives for this payload on the HASP flight, the concept of operation, the enabling hardware platform for this research, and a combination results/failure analysis for the 2012 flight.

II. Science objectives

II. a. Radiation sensor testing

The primary science objective for this flight was to demonstrate the functionality of the radiation sensor in a near-space environment. The high altitude and extended duration of the HASP flight offered a unique opportunity to test the sensor under exposure to cosmic radiation. The chance of observing strikes by radiation with enough energy to pass fully through the sensor was increased by the long flight duration. Particles which pass completely through the 300-µm thickness of the sensor are of particular importance because they register in the high-speed sampling circuitry as intersections of front and back-side sensor channels. Strikes which only register on a front side channel are assumed not to have passed through the sensor, and therefore they do not pose a threat to the computer system. Data from intersection strikes, including the rate at which they occur, can subsequently be input into fault injection simulations to extract worst-case scenario performance statistics of radiation-tolerant computer architectures. Neutrons were expected to be the predominant particles encountered as they represent the bulk of energetic particles in the atmosphere (1). The atmospheric neutron flux is well known (2) and a major test of the sensor was to replicate the neutron flux profile during the ascent phase of the flight. The desired data products included the ionizing radiation strike rate (particles/s), sensor spatial strike information, and particle flux (particles/cm^2/s).

II. b. SEE detection in SRAM FPGAs

A secondary science objective was to detect single event effects within either of the two FPGAs in the payload. This objective required the complete design and development of the radiation-tolerant architecture test platform. The FPGA board was designed to include two FPGAs: a control FPGA, and a general-purpose, high-performance computational-resource FPGA. The control FPGA, a Xilinx Spartan-6 (XC6SLX75), acted as a system controller as it housed the high-speed sampler for the radiation sensor, controlled the communication between the payload and the HASP platform, and controlled the configuration and operation of the computational FPGA. The computational FPGA was a Xilinx Virtex-6 (XC6VLX75T-1L). Since the majority of development time was devoted to designing the requisite circuit boards, a complete radiation-tolerant architecture was not implemented for testing on this flight. Instead, a detection system was implemented which allowed SEUs and SEFIs to be identified and avoided, but not repaired. This was viewed as an initial step toward the implementation of a fully-functional radiation-tolerant system.

For the HASP 2012 flight, the Spartan-6 device used a dedicated, internal CRC hardware

component on the configuration memory, which was input into the control microprocessor as an interrupt to indicate fault occurrence. The SEE detection strategy for the Virtex-6 used an array of 16 Microblaze processors with three running at a time (triple modular redundancy, or TMR). The outputs of the processors were sent to a majority voter, which determined if any of the active processors were faulted. The system would replace faulted processors with one of the available spares. Signals representing the set of active processors were sent to the Spartan-6. Single event effects could thus be observed through changes in the active processor set in the Virtex-6.

II. c. Thermal performance

A third science objective, which evolved over the life of the project, was to determine the thermal behavior of the electronics in a low-pressure environment. The payload electronics were under development for the majority of the project life. This precluded early thermal testing to see if the system would overheat, or cool excessively during ascent and float. Simulations were relied upon to provide estimates of the thermal behavior of the system. These models included finite element analyses of the combined electronics, mounting hardware, and enclosure as well as component-level models derived from the PCB layout. Initial FEA simulations indicated that the payload would easily exceed the +100˚C maximum operating temperature of the FPGAs. These models informed the design of the payload enclosure and motivated several important PCB design decisions, which will be detailed in a subsequent section. After refinement, the models were within 10˚C of the observed payload temperatures both at integration and during flight. The payload enclosure was designed with the main goal of maintaining FPGA core temperatures within their specified operating ranges. The inability to cool the electronics using convective processes complicated the design. A combination of conduction and radiative cooling were used to move heat away from the electronics and radiate it externally.

III. Concept of Operation

The payload was designed for autonomous flight operation with minimal administrative commands. At power-on, the system performed an initialization sequence during which the FPGAs were configured, the control processor was booted, and the data storage structures were initialized. A Microblaze soft processor was used to control the system. Its operation was interrupt-driven as it handled receipt of commands and GPS data from the HASP platform, and transmitted raw telemetry data at each expiry of a 20-second fixed-interval timer. Transmitted data included a system counter, which served as a heartbeat to show that the system was running, the number of cumulative counts

observed on each channel of the radiation sensor, the junction temperature of the Virtex-6 FPGA, GPS time and position data, single event effects data, and system status flags.

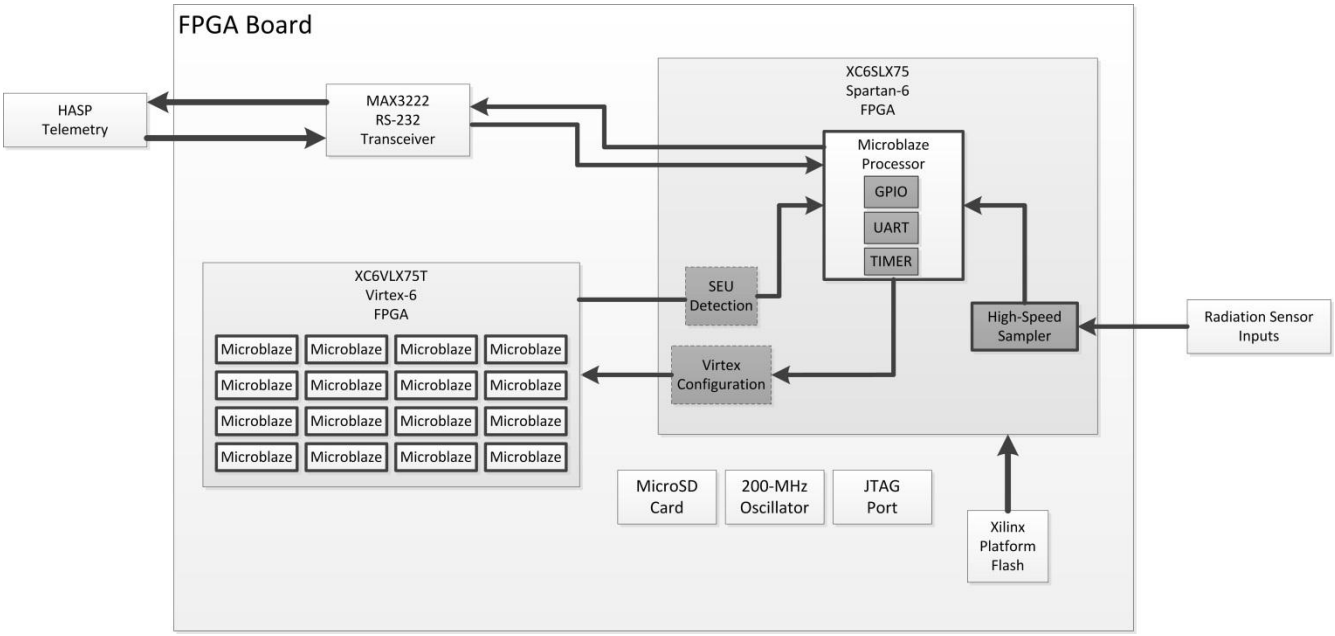

Figure 2- FPGA CCA architecture. This figure shows 16 Microblaze processors instantiated on the Virtex-6, the RS-232 interface to the HASP platform, and the major components of the Microblaze processor on the Spartan-6 FPGA.

The data were retrieved from the HASP website as it became available during the flight. After retrieval, the data were processed in MATLAB and the contents of each telemetry packet were displayed on a graphical user interface. This gave the team the ability to scroll through all the received packets to determine how the system was operating. Two payload commands were available to the team during the flight. These were commands to reset the radiation sensor counters and to reconfigure the Virtex-6. The primary job of the team during the flight was to make sure the payload was transmitting data as expected. If the data transmission ceased, as it did twice during the flight, a power cycle would be requested to re-start the payload.

IV. System Hardware

IV. a. Power CCA

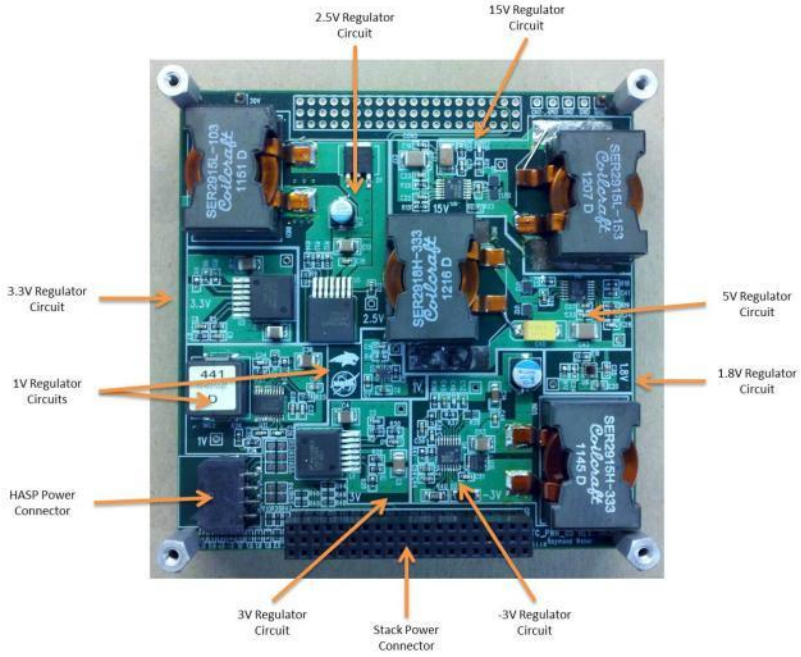

Figure 3- Power CCA designed for the HASP 2012 flight.

Power was supplied to the payload via the HASP interface. The Power CCA, shown in figure 3 generated the required internal system voltages from the provided 30±2 volt supply. Given the strict power consumption restrictions the system was designed using high-efficiency DC-DC converters. This minimized the amount of the payload power budget consumed by the conversion process. A secondary benefit of efficient power conversion is a reduction in generated heat as compared to linear regulators. The FPGA CCA and sensor electronics combined to require 8 voltage rails and 1 additional intermediate rail to increase efficiency. An estimated payload power dissipation of 6.2 watts was calculated during the design process. The measured power consumption at payload integration was 6.5 watts. Fitting this number of regulator circuits on the 4-in x 4-in PCB required extremely careful design work. A diagram detailing the conversion architecture is shown in figure 4.

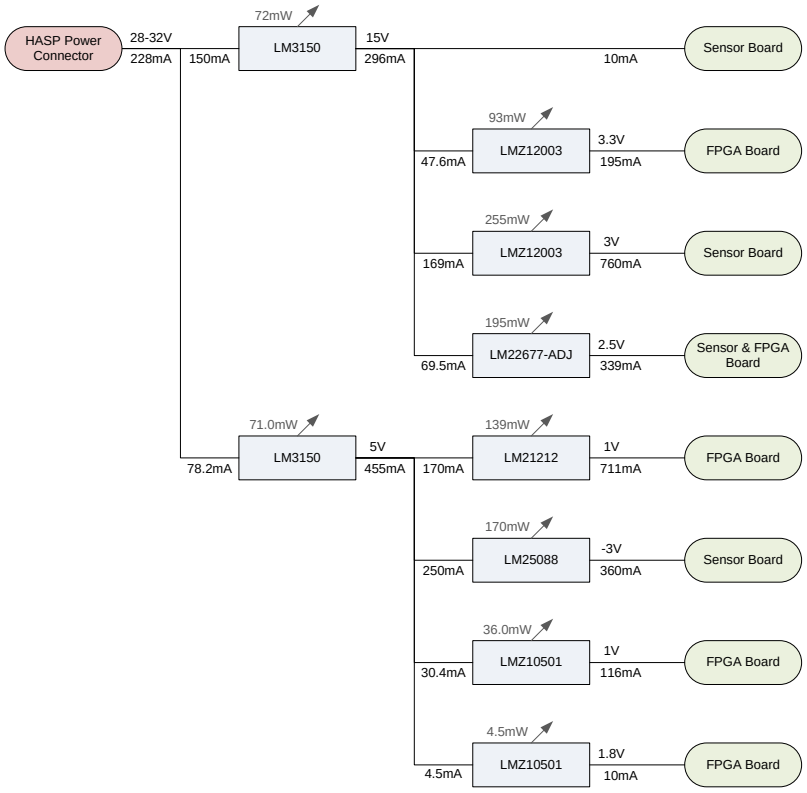

Figure 4- Power conversion diagram.

IV. b. FPGA CCA

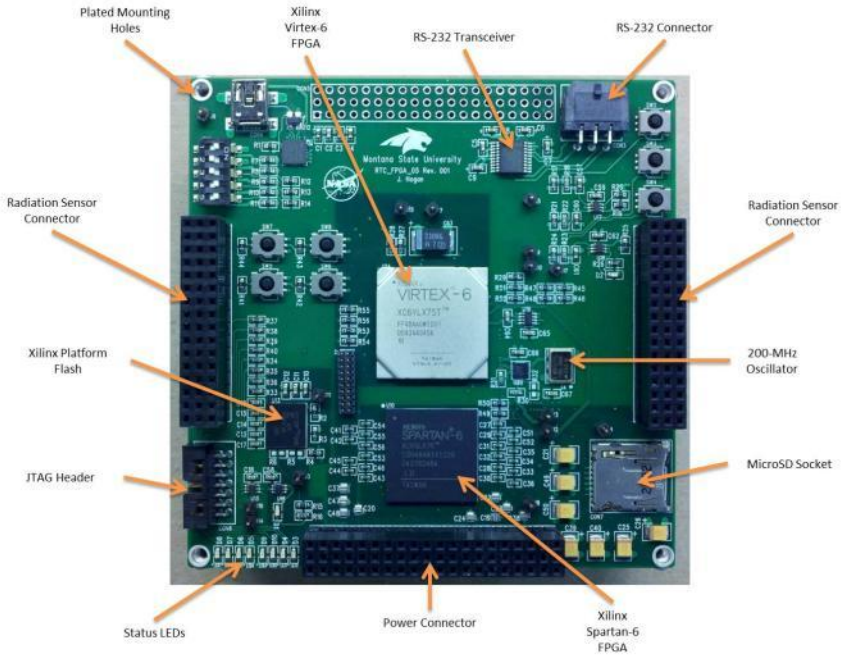

Figure 5- FPGA CCA designed for the HASP 2012 flight.

The FPGA circuit card assembly served as the system controller for the flight. Upon application of power to the payload, the Spartan-6 FPGA self-configured using an 8-bit SelectMAP Master interface to a 32-Mbit configuration memory device. The Spartan-6 FPGA contained three major hardware components: an SD card controller, a Microblaze soft processor, and the high-speed radiation sensor sampling logic. Immediately after configuration, the SD card controller performed an initialization sequence on the SD card to allow access to it via an SPI interface. The SD card was pre-loaded with the configuration bitstream for the Virtex-6. Once the SD card initialization process was complete, control of the card was handed over to the processor. The first task of the processor was to read the configuration data from the SD card and write it to the Virtex-6 via an 8-bit SelectMAP Slave interface. Upon completion of the configuration process, the processor began data collection operation. The process was interrupt driven and had service routines for the following tasks: read commands and GPS data from the HASP RS-232 interface, transmit command receipt acknowledgments to the HASP RS-232 interface, record CRC error in configuration memory contents, and transmit telemetry packet every 20 seconds. As part of the telemetry transmission task, the processor would read the most recent GPS location and time data, the junction temperature of the Virtex-6 and the contents of the radiation sensor sampler memory. Each valid telemetry packet was 1224 bytes long including a header, footer, checksum, and all data contents.

IV. c. Sensor CCA

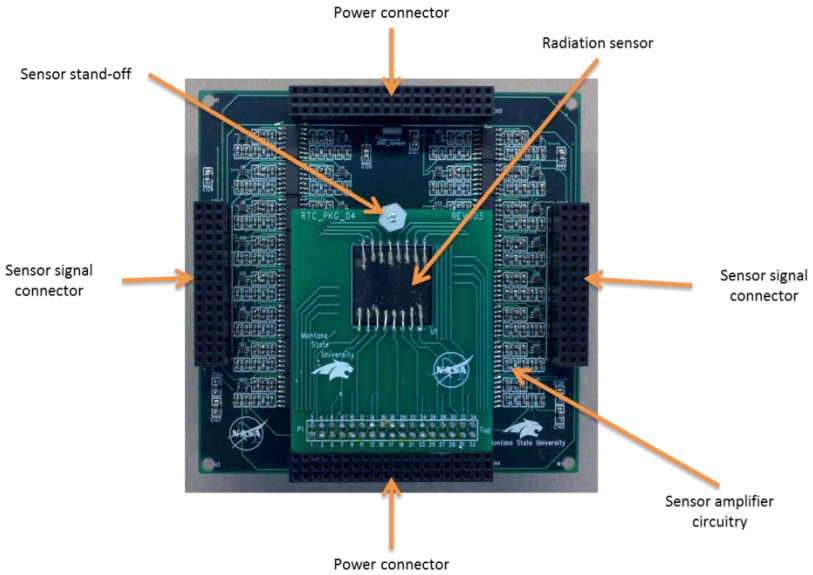

Figure 6- Radiation sensor CCA. The CCA includes the radiation sensor, sensor signal breakout board, and signal conditioning electronics.

The radiation sensor CCA consists of a custom silicon strip sensor and a chain of amplifiers used to condition the analog sensor outputs into a square pulse. The radiation sensor is a silicon-based strip detector. The substrate consists of an intrinsic silicon wafer with a P-type (Boron doped) front surface and an N-type (Phosphorous doped) rear surface. These doped regions produce an inherent electric field inside of the silicon sensor. When a heavy radiation particle penetrates the sensor, bonds between electrons and host atoms are broken. The breaking of these bonds produces free electrons inside the substrate. The movement of these electrons effectively produces two types of charge carriers. The electrons themselves are the first carrier. The second carrier is represented by the void left by a traveling electron and is known as a hole. The combination of the traveling electrons and holes produces the desired signals. Once these carriers are generated, they are separated by the internal electric field inside the sensor. The electrons are pushed to the rear of the sensor while the holes move towards the front. These transient signals are then collected from the front and rear aluminum electrodes. The signals are input into a two-amplifier chain which amplifies and stretches the pulse for input into the high-speed sampler located in the Spartan-6. The high-speed sampler is a rising-edge triggered system which functions as a counter for each of the radiation sensor channels.

IV. d. Electronics Stack

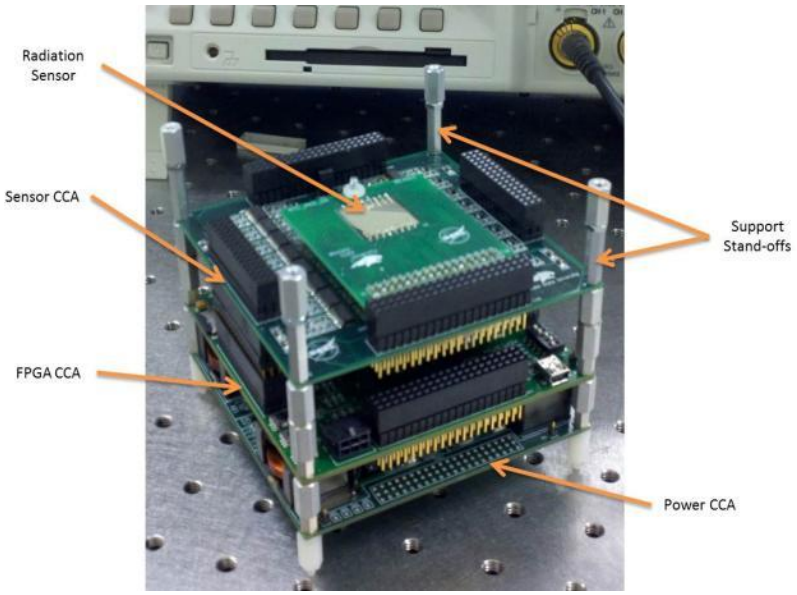

Figure 7 - Payload electronics stack.

The payload electronics stack consisted of a Power CCA, an FPGA CCA and a Sensor CCA. The

circuit boards were stacked together using through-hole connectors and secured using threaded aluminum stand-offs at each corner. In addition to providing mechanical support these stand-offs were part of the payload thermal solution. The mounting holes on the FPGA and Power CCAs were plated and connected to the internal ground planes. This allowed heat to flow through the PCB ground planes to the aluminum stand-offs. A 4x4x1/8-in copper plate was placed at the bottom of the payload, secured using the stand-offs, and used as a heat sink during flight. Thermal models indicated this was a good solution for maintaining the desired operating conditions, and the payload encountered no thermal issues during payload integration or flight.

IV. e. Enclosure

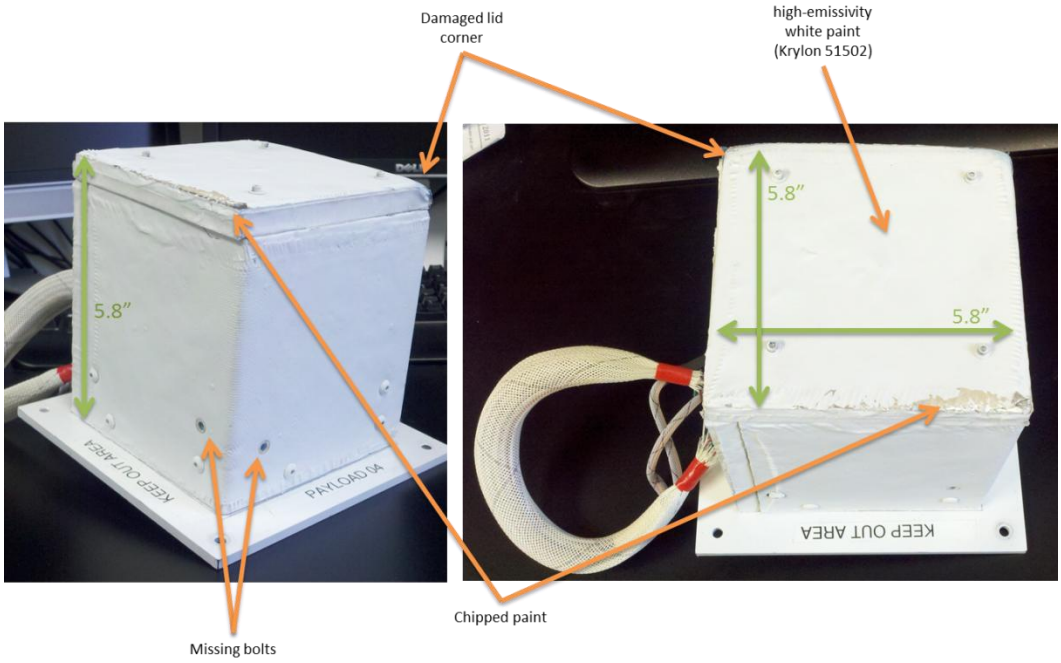

Figure 8- Payload enclosure. The enclosure was made of half-inch thick foam insulation wrapped in a thin sheet of aluminum foil. A fiberglass layer was added for structural support. The enclosure was painted using Krylon Indoor/Outdoor Flat White spray paint (#51502).

The enclosure was designed for thermal and mechanical protection of the payload electronics. The approach to thermal protection sought to maximize reflection of solar irradiation using a thin layer of aluminum and a flat, high-emissivity white paint. Beneath the aluminum layer was a half-inch of insulating foam material, which minimized heat transfer between the enclosure and the outside

environment. Within the enclosure, the heat generated by the electronics was conducted away from sensitive components through PCB ground planes, into aluminum support stand-offs, and into a copper heatsink. The heatsink was placed inside the enclosure, beneath a piece of insulating foam to prevent internal radiative heat transfer. The bottom of the heatsink was in contact with the PVC mounting plate. Though not an excellent thermal conductor, it was expected that this configuration would heat the mounting plate allowing a moderate amount of heat to be radiated from the payload toward the earth. The electronics stack and enclosure were attached to the mounting plate separately. The electronics stack was secured by screws which engaged the threaded aluminum stand-offs. The enclosure was held in place using bolts and nuts which affixed internal angle brackets to the mounting plate. The enclosure survived the flight reasonably well. Damages to the payload between launch and return shipment receipt included chipped paint on the enclosure lid, a smashed corner on the lid, two missing side-panel bolts, and one sheared-off nylon stand-off, which was helping to hold the lid down. Evidence of strain was visible on the remaining 3 nylon stand-offs.

V. Results

The following table provides an events timeline for the payload during the flight. The two most notable events are anomalies 1 and 2. In these events, the payload failed to operate properly and required a power cycle to restore function. The delay in the availability of telemetry data and communicating the need for a power cycle with HASP operators led to extended downtime during each of the failures. Other events include GPS dropouts of varying duration resulting in loss of time and payload position data.

Event	Time (MDT)	Description
Initial Power-On	07:45	Payload turned on for flight
First Data Packet Received	07:45:46	
Launch	08:19	
GPS Data Invalid	08:51 – 09:00	GPS fix invalid
GPS Data Invalid	09:54 – 10:24	GPS fix invalid
Payload Anomaly #1	10:25	36-minute shutdown
Float Start	10:28	Balloon reached float altitude
Restart #1	11:01	Payload successfully restarted
Payload Anomaly #2	11:30	1-hr 34-minute shutdown
Restart #2	13:04	Payload successfully restarted
Power-Down #1	18:19	Payload power turned off
Power-On #1	18:22	Payload power restored
Last Data Packet	19:01	
Flight Termination	19:17	
Impact	20:07	HASP platform back on the ground

Table 1 - Major events during the flight.

As the data became available during the flight it was processed and viewed in a custom MATLAB telemetry GUI. This GUI provided a graphical display of the radiation sensor including the number of cumulative strikes at each of the 256 intersections. In addition to the radiation sensor data, the GUI displayed the contents of the most recent telemetry packet. This included the system heartbeat counter, UTC time, latitude, longitude, altitude, GPS fix status, a payload start status word, the set of active processors on the Virtex-6 and the Virtex-6 junction temperature. Figure 9 below shows the data processing GUI.

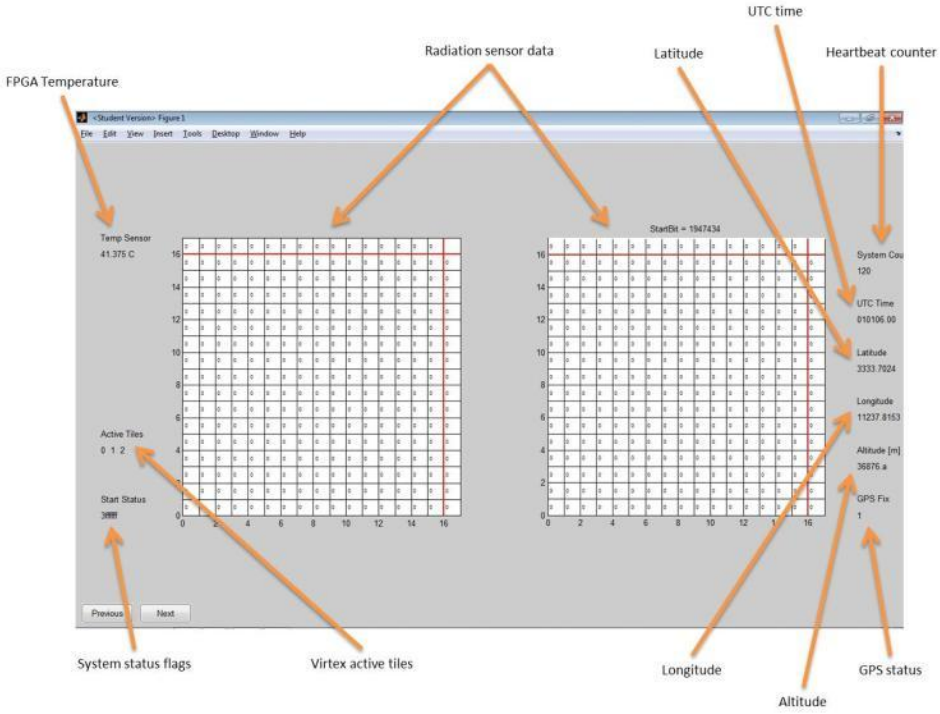

Figure 9- This figure shows the data processing GUI used during the flight. The presentation of the telemetry data simplified the monitoring of payload operation.

The payload was observed to be operating nominally upon initial power up the morning of the flight. Shortly after launch, during the ascent phase, it became apparent that the radiation sensor was not appropriately sensitive as it recorded no radiation strikes on the way to float altitude. Proper payload operation was demonstrated by the validity of the other downlinked data, so it was hypothesized that something related to the sensor was preventing strikes from being observed. Unfortunately, the payload failed to record the desired radiation data for the duration of the flight.

The SEE detection circuitry worked throughout the flight without detecting any events. This scientific objective was considered secondary science due to the small, though non-zero, chance of observing an upset in a sensitive bit within either of the FPGAs. The chance of upset was considered small due to the low SEU cross-section of the FPGAs (on the order of 10^{-9} cm^2/bit) (3) as well as the expected low bit error rate. Bit error rates are low because of the combination of a negative correlation of particle flux with particle energy and small radiation cross-section of the devices. Only a handful of particles with sufficient energy to induce an upset were expected to be encountered during the flight, and these particles needed to strike the FPGA substrate in very specific locations to be observed. The effects of high-energy particles on avionics is well known (2,4,5,6), so with this flight hardware an

attempt was made to detect these effects despite the low probability of occurrence.

The thermal data from the flight was undoubtedly the most useful result obtained. Though it was not the main objective, these data represent very important performance characterizations for this computer system. The system had never been operated in a low-pressure environment and there was uncertainty about its ability to survive the thermal rigors of the flight. Looking forward, this information provides a good understanding of what to expect for future flights as it is anticipated that a slightly modified system will be flown on another high-altitude balloon, hopefully HASP, as well as into space on a sub-orbital launch vehicle.

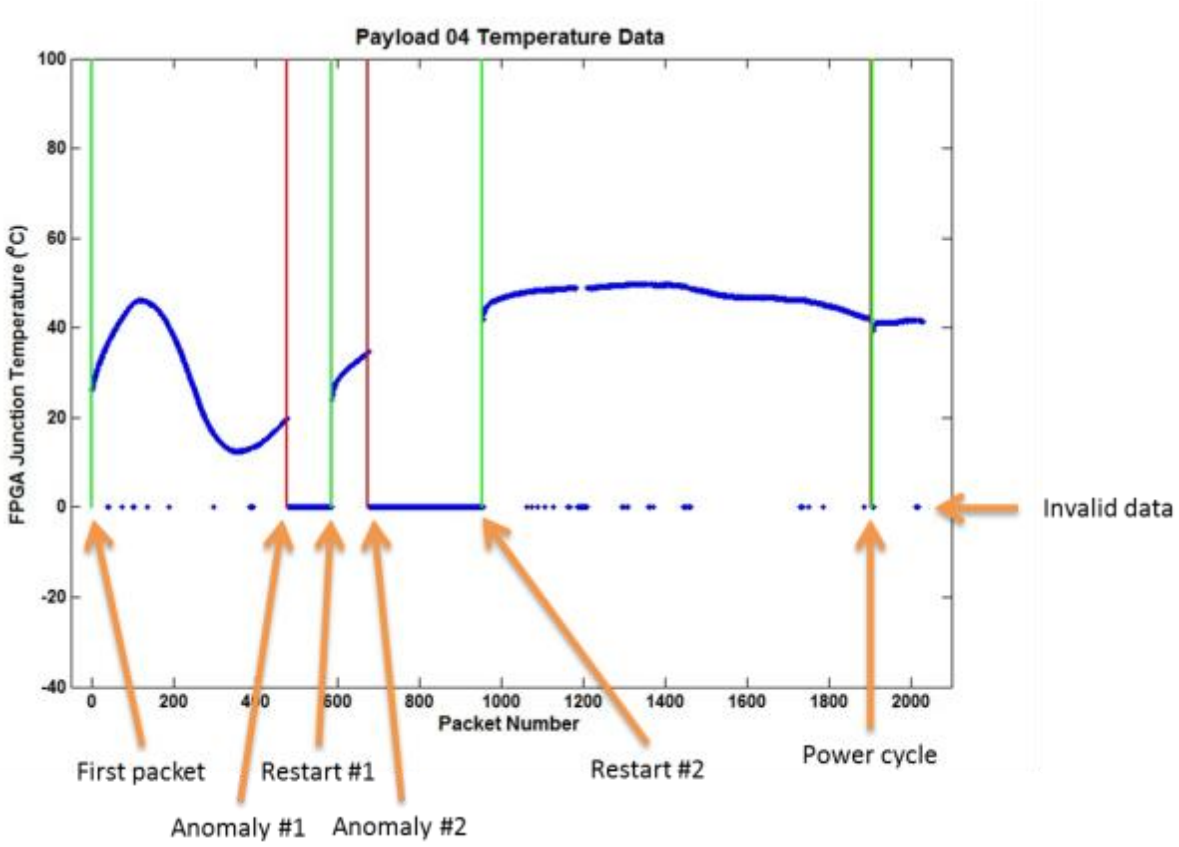

Figure 10- This plot shows the Virtex-6 FPGA junction temperature during the flight. The maximum observed temperature was 49.8 ^{o}C, and the minimum was 12.4 ^{o}C. The payload stayed within the -40^{o}C to 100 ^{o}C operating limits.

Though there was no immediate use for the position data obtained during the flight, it was interesting to see it plotted and to look at the track the balloon took from launch to landing. The

latitude, longitude, and altitude data were imported into Google Earth for a 3-D mapping of the flight path. Portions of the flight during which the GPS fix became invalid are visible in the data. The figure below shows the full track of the flight along with the elevation profile along the bottom.

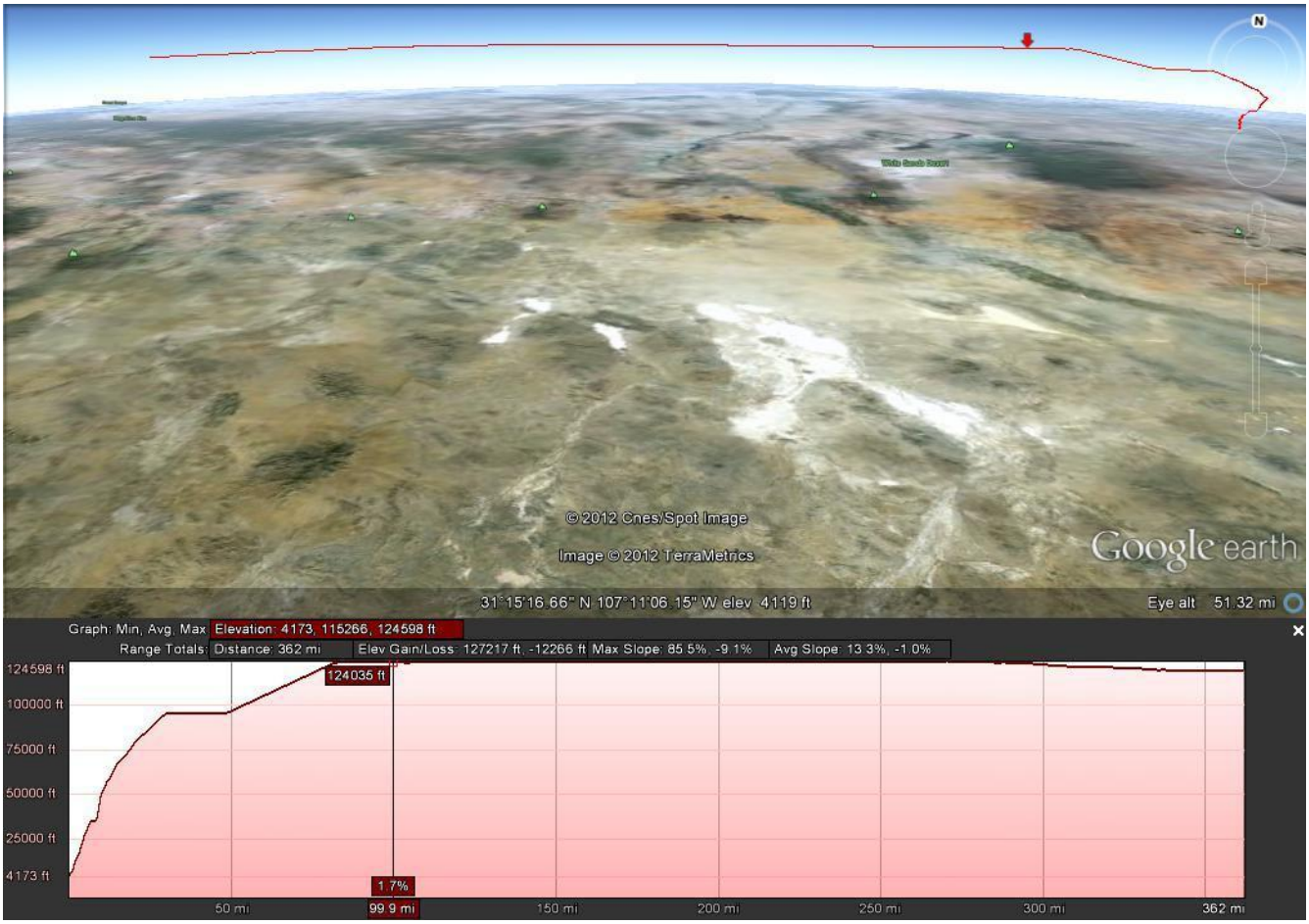

Figure 11 - Google Earth rendering of the 2012 HASP flight track.

VI. Failure Analysis

VI. a. Power supply failure

Prior to flight, the sensor and amplifier board were tested for functionality in two ways. The first, which was used mainly to demonstrate spatial sensitivity and to expose broken sensor channels, used a pulsed 5-mW 980-nm laser. Pulse widths down to 20-ns were achieved using an acousto-optic modulator (AOM) triggered at a pulse repetition rate of 1-Hz. Results of these tests gave confidence that the flight sensor was functioning as expected.

The second functionality test of the sensor involved exposure to high-energy ions at the Texas A&M

Radiation Effects Facility. In these tests, the sensor and amplifier board were tested in a ~25 MeV/AMU Krypton beam. For data acquisition, the sensor CCA was attached to a development board rather than the flight FPGA board because the FPGA CCA had not yet been manufactured. These tests demonstrated that the flight sensor and amplifiers were sensitive at least down to 25 MeV.

After the FPGA CCA board was built and tested, the full system was tabletop tested using a 650-nm red laser pointer and a 980-nm near infrared laser pointer to stimulate the radiation sensor. These tests gave confidence that the radiation sensor was working properly with both the power board and the FPGA board. However, events during the flight and subsequent testing demonstrated this to be wrong.

Two operation anomalies were observed during the flight. In these events, the payload continuously streamed data beyond the typical 1224 byte packet length (up to ~8000 bytes) before becoming unresponsive. These events were investigated during post flight testing of the hardware to determine what caused the system to crash unexpectedly. The aforementioned low-power pulsed laser setup was used to perform the tests. This round of testing included the entire electronics stack used during flight. The sensor was stimulated with pulses of varying width at a 1-Hz repetition rate. The failure behavior was successfully replicated by increasing the pulse width to about 170-µs at which point the system began to stream data continuously prior to freezing. An audible tick sound was observed coming from the power supply circuitry with each incident laser pulse. This was a result of the power supply's inability to handle the current transients associated with the voltage level switches occurring in the sensor amplifier circuitry. These transients, in turn, caused instability in the voltage regulators due to insufficient phase margin in the regulator feedback path. The amplifiers drew unexpectedly high currents during pulse strikes peaking at a maximum of 1.5A. This peak was up from a nominal value of 0.15A on -3V and +3V. When combined with other EMI issues present on the CCA (coupling between regulator circuits), these transients caused both intermediate voltage rails (+5V and +15V) to collapse, and thus the core FPGA voltage rails to also collapse. This resulting power glitch was sufficient to cause the FPGA to lose programming/configuration, but wasn't long enough to trigger a full system reset. The result was erratic payload behavior followed by a freezing of the control processor. Figure 11 shows the Spartan-6 core voltage dropping below the 800-mV limit after which FPGA configuration memory is corrupted.

In summary, the power supply system flown on the HASP 2012 flight was unable to handle current transients induced by radiation strikes to the sensor. Insufficient phase margin in regulator feedback loops combined with excessive coupling between regulator circuits caused instability in and subsequent collapse of critical system voltage rails. This rail collapse led to loss of FPGA configuration resulting

in payload malfunction. These problems have been addressed and fixed in a second revision of the power supply system. This new power supply CCA has been designed and is under test at the time of this writing. No problems with the new, more robust power supply system have been found.

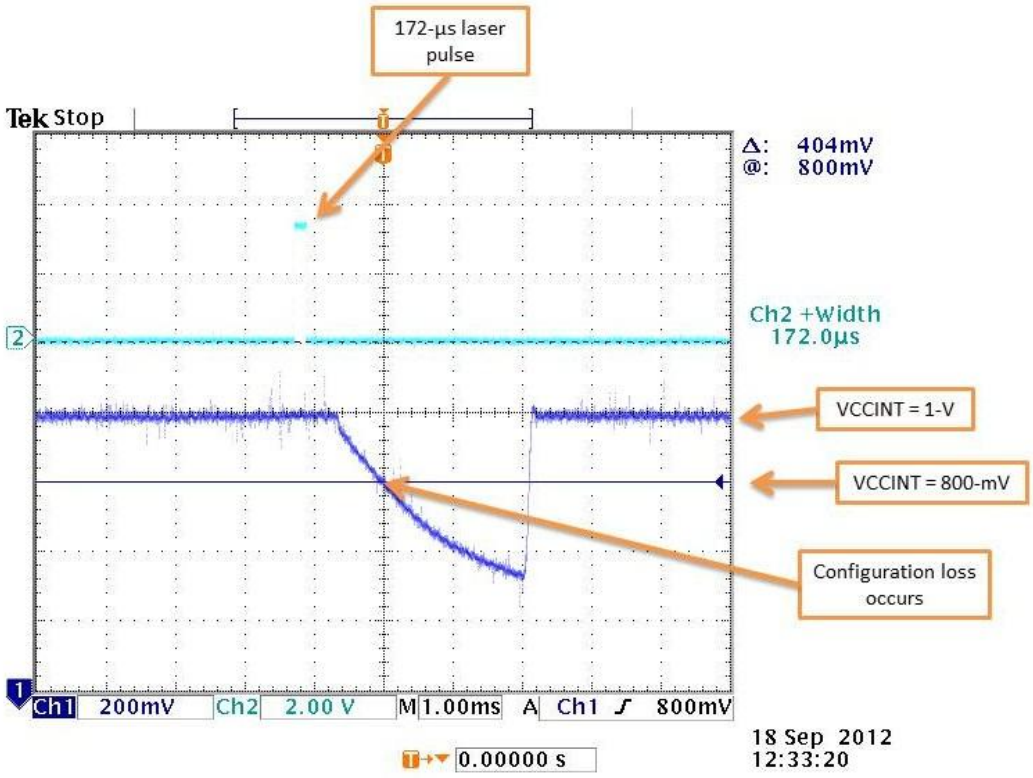

Figure 12- Laser-induced system failure. This failure replicates the observed failure behavior during the flight. It is hypothesized that the most likely causes of the two observed failures were multiple-channel radiation strikes.

VI. b. Excessive shielding and inadequate gain

Part of the primary science was to measure the atmospheric particle flux profile. It is evident from the power supply failure analysis that this goal was unachievable with the flight hardware. The analysis showed that for each radiation strike the system could reasonably be expected to crash. If the radiation sensor was sufficiently sensitive to measure the atmospheric particle flux profile, it is expected that the system would have crashed much more often than it did. With a peak neutron flux alone estimated at 4 n/s incident on the sensor (4), it is suspected that the payload as flown was not sensitive to much of the lower energy portion of the radiation environment. There are two contributing

factors to this lack of sensitivity: aluminum layer on payload exterior shielded low energy particles, and insufficient gain on the radiation sensor signal conditioning amplifiers prevented detection of highly-penetrating low-energy neutrons. For measuring the atmospheric radiation profile it is important that the sensor be sensitive to the low energy part of the radiation spectrum since that is where the highest fluxes are found. Before future flights closer study of the appropriate gains will be conducted. This will ensure that the payload is sensitive enough to measure the much more active parts of the atmosphere during a flight.

VI. c. Extraterrestrial activity

Leaving no stone unturned in the post-flight search for system failure explanations it is important to note multiple reports of extraterrestrial activity in the vicinity of the HASP balloon near the end of the flight. These reports originated out of the greater Phoenix metro area (7,8), and make reference to a self-cloning "mother-orb" (9,10). Without a better understanding of the technological capabilities of these presumably complex, exotic interstellar flight vehicles it is impossible to say what effect, if any, they would have on payload performance.

VII. Team members and demographics

VII. a. Participant demographics

Name	Gender	Ethnicity	Race	Student Status	Disability
Emily Bishop	Female	non-Hispanic	Caucasian	Undergraduate	No
Todd Buerkle	Male	non-Hispanic	Caucasian	Graduate	No
Elizabeth Clem	Female	non-Hispanic	Caucasian	Undergraduate	No
Blaine Ferris	Male	non-Hispanic	Caucasian	Undergraduate	No
Jennifer Hane	Female	non-Hispanic	Caucasian	Graduate	No
Justin Hogan	Male	non-Hispanic	Caucasian	Graduate	No
Adrien Lambert	Male	non-Hispanic	Caucasian	Graduate	No
Raymond Weber	Male	non-Hispanic	Caucasian	Graduate	No
Kaysha Young	Female	non-Hispanic	Caucasian	Graduate	No

VII. b. Recent graduates

Todd Buerkle – MSEE, May 2012, Micron Semiconductor, Product Engineer

Elizabeth Clem – BS Mechanical Engineering Technology, May 2012, employment unknown.

Jennifer Hane – MSEE, May 2012, Seakr Engineering, FPGA Engineer

Adrien Lambert – MSME, December 2012, employment unknown

VIII. References

[1] C. S. Dyer and P. R. Truscott, "Cosmic radiation effects on avionics," *Microprocessors and Microsystems*, vol. 22, pp. 477-483, 1999.

[2] E. Normand and T. J. Baker, "Altitude and Latitude Variations in Avionics SEU and Atmospheric Neutron Flux," *IEEE Trans. Nucl. Sci.*, vol. 40, p. 1484, Dec. 1993.

[3] D. M. Hiemstra and V. Kirischian, "Single Event Upset Characterization of the Virtex-6 Field Programmable Gate Array Using Proton Irradiation," IEEE Radiation Effects Data Workshop, 2012.

[4] A. Taber and E. Normand, "Single Event Upset in Avionics," *IEEE Trans. Nucl. Sci.*, vol. 40 no. 2, p. 120, April 1993.

[5] E. Normand, "Single-Event Effects in Avionics," *IEEE Trans. Nucl. Sci.*, vol. 43 no. 2, p. 461, April 1996.

[6] A.H. Johnston, G. M. Swift, and L. D. Edmonds, "Latchup in Integrated Circuits from Energetic Protons," *IEEE Trans. Nucl. Sci.*, vol. 44 no. 6, p. 2367, Dec. 1997.

[7] http://www.abc15.com/dpp/news/region_phoenix_metro/central_phoenix/valley-residents-observe-ufo-saturday-evening

[8] http://www.myfoxphoenix.com/story/19437737/strange-balloon-launched-by-weather-service

[9] http://www.ufosightingsdaily.com/2012/09/ufo-over-phoenix-arizona-during-daytime.html

[10] http://policecosmiccode.blogspot.com/2012/09/ufo-in-phoenix.html